Experimental analysis of the evolution of the physical properties of pyramidal-shaped metallic replicas made using the MIM process

Jie Zhang, Mohamed Lakdhar Sahli, Jean-Claude Gelin, Chantal Khan-Malek

Experimental analysis of the evolution of the physical properties of pyramidal-shaped metallic replicas made using the MIM process

J. Zhang & M. Sahli & J.-C. Gelin & C. Khan-Malek

Abstract In the applications of powder injection moulding (PIM), the metallic powders are the most popular material. In our study, three metallic powders with different compositions, particle shapes and particle sizes have been selected as the test materials to produce micro-structured parts using injection moulding process. The combination of three binders (polypropylene, paraffin waxes and stearic acid) with a constant and adapted formulation has been chosen as a binder system. The mixtures obtained by mixing the metallic powders and the binder system with solid loadings ranging from 56 to 64 vol.% have been used as the feedstocks for the next injection moulding. The viscosity of mixture increased with increasing solid loading. These feedstocks were injected using the same injection moulding conditions in the metallic mould structured with pyramidal shape manufactured using electro-erosion machining. The debinding and sintering process have been carried out at different temperatures to eliminate the binders in the injected replica and obtain the final metallic die mould. To analyse the physical properties evolution of the die mould manufactured by PIM and the influence factors (powder nuance, solid loading and sintering conditions), the shrinkage rate, density, roughness of surface, Vickers hardness and mass losses in metallic mould cavities were investigated. The experimental results demonstrate that properly micro-structured parts can be obtained using the process chain of injection, debinding and sintering with metallic powders.

J. Zhang · M. Sahli · J.-C. Gelin
Applied Mechanics Department, Femto-ST Institute,
CNRS UMR 6174, ENSMM, 26 rue de l'épitaphe,
25030, Besançon Cedex, France

J. Zhang (✉) · C. Khan-Malek
MN2S Department, Femto-ST Institute, CNRS UMR 6174,
32 Avenue de l'Observatoire,
25044, Besançon Cedex, France
e-mail: jie.zhang@femto-st.fr

Keywords Injection moulding · Metallic powders · Sintering · Thermogravimetric analysis · Viscosity

1 Introduction

Powder injection moulding (PIM) is an attractive manufacturing technology for processing metal, ceramic and glass powders into desired components with near-net shape. PIM combines plastic injection moulding and powder metallurgy processes, thence PIM has their both advantages including: low fabrication cost, mass production, high complexity of part shape, great diversity of materials and high geometrical accuracy [1–5]. The conventional PIM process consists of four main steps: mixing, injection moulding, debinding and sintering, as illustrated in Fig. 1 [6–8]. First, a binder system with a suitable formulation is mixed with a fine powder to obtain a homogeneous feedstock. The binder is a key component which provides the powder with a low viscosity for easy filling of the micro-cavities and a good formability for moulding during the injection moulding process [9–11]. Afterwards, the prepared feedstock is transformed into solid pellets by a granulation process and then injected to get the polymer/powder parts with the required shapes. After the injection moulding, the debinding and sintering processes are conducted respectively to eliminate binders from the moulded parts and to obtain the final densification of the products with required properties by solid-state diffusion [12, 13].

In the PIM, the metallic powder is the most popular material because of its good mechanical and electrical properties; moreover, the metallic components manufactured by PIM have a wide application including automotive industry, electronics, medical technology, and biotechnology; therefore, a branch of PIM–metal injection moulding (MIM) has been paid a much attention.

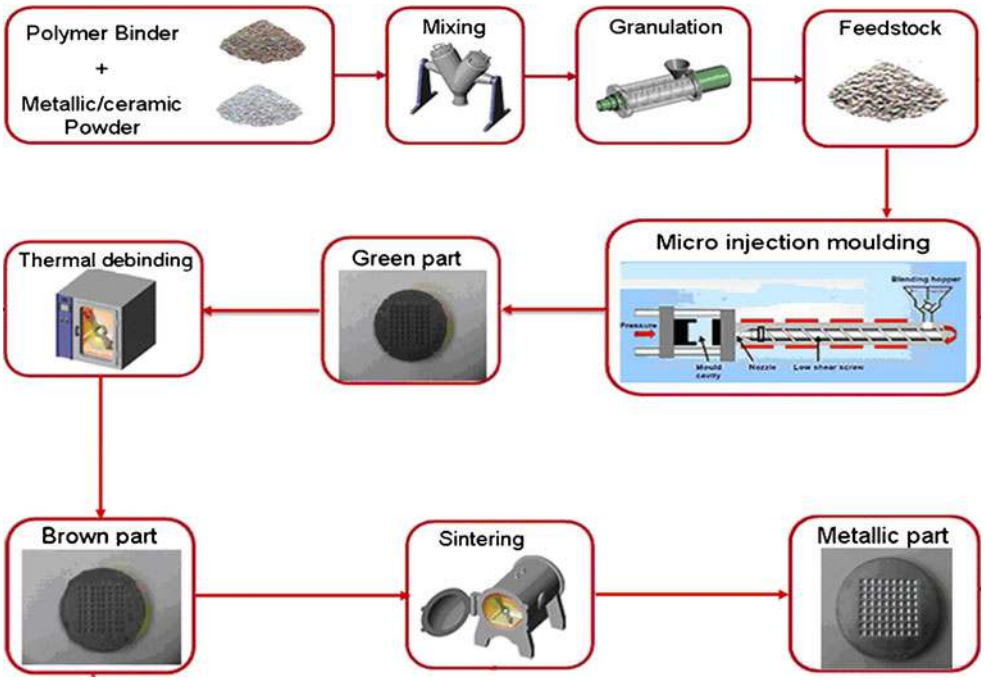

Fig. 1 Schematic process flow for rapid manufacturing of die mould from metallic powders

For the MIM, different factors in every step of manufacturing process can affect the final quality and physical properties of the products, due to the complexity of the process. To obtain the better quality of products and achieve the control to the fabrication process, a lot of investigation works has been carried out around the manufacturing process, material properties, process impact factors, and product properties [14–19]. For example, Li et al. [20] investigated the processing steps for producing 440C stainless steel parts by means of powder injection moulding technique. It is observed that the effective densification took place in the temperature range 1,230–1,240 °C in the sintering process and too high sintering temperature will result in a rapid grain growth, slumping, nonuniform densification, pore coalescence and swelling. After heat treatment, the micro-structure of injection moulding 440C stainless steel consisted of martensite, residual austenite, carbide and specimens sintered at 1,240 °C for 30 min have the tensile strength of 876.3 MPa and the hardness of 57.7 HRC. Besides, they found also that the content of carbon has heavily affects ion on the shape retention. Some methods, such as preventing from oxidation, are presented to avoid the as-sintered specimens from deformation. Khalil et al. [21] have studied the mechanical properties and micro-structures of 17-4ph stainless steel parts produced using different binder contents (solid loading) by powder injection molding (PIM) process, it is demonstrated that the high performance properties, such as fully dense, ultimate tensile strength, hardness, and wear resistance are obtained with high solid loading. Okubo et al. [22] investigated the effects of particle size and distribution of metal powder on dimensional accuracy of micro-dumbbell specimens at both grip parts. Powders of stainless steel 316 L and 17-4PH with three different particle sizes and distributions were used in the study. By evaluating the relationship of dimensional accuracy and powder property, they found that stabilisation for high material must be added to MIM compounds for reducing the flow ability and dimensional accuracy can be improved with downsizing the particle size. Moreover, optimum sintering temperature is existed in sintering process. Relation of dimensional accuracy and sintered density were considered to be very important in sintering process. Li et al. [23] investigated the effects of the solid loading on the feedstock rheological properties, the compact distortion and tolerance control as well as the mechanical properties and microstructures. It is proved that the feedstock with 68 % solid loading can be injection moulded with a comparatively low viscosity on a relatively wide temperature range. Besides it is best to get quick powder re-packing and binder molecule orientation during injection moulding. Finally it is easy to get sintering densification and obtain the sintered components with superior mechanical properties and proper microstructures using this feedstock of 68 % solid loading in PIM process. Choi et al. [24] investigated the effect of sintering conditions on the properties of WC–10 wt.% Co PIM compacts, they found that: in the case of those sintered at 1,380 °C in vacuum atmosphere, the hardness was 1,600 Hv, and the

Table 1 Particles size distribution of different powders

Powders	Diameter (μm)	D_{10} (μm)	D_{50} (μm)	D_{90} (μm)	Density (g cm^{-3})
316L stainless steel	3.5	1.8	3.4	6.0	7.90
	16	4.1	3.4	6.0	7.90
Fe–Ni (8 %)	5	2.4	4.4	8.0	7.93

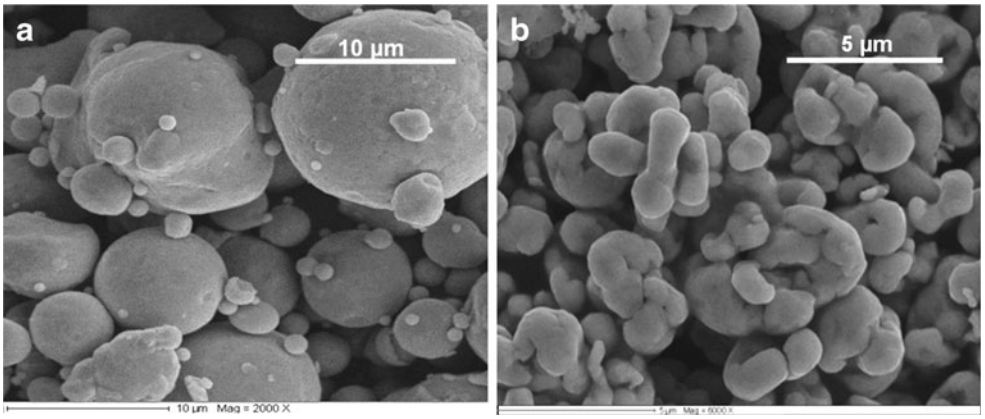

Fig. 2 SEM photographs showing: **a** 316L stainless steel powders (16 µm) and **b** Fe–Ni powders of 5 µm

relative density of WC–10 % Co was 92.5 %. The density of WC–10 wt.% Co sintered at 1,380 °C in mixed gas atmosphere was 87.5 % and the hardness was lower than 1,400 Hv. Residual carbon contents of sintered at vacuum and mixed gas atmosphere were 5.4 wt.%.

In this paper, the aim of the work is to investigate and analyse the evolution of physical properties of a die mould manufactured by MIM as well as the influence factors. To MIM process, the experimental study has consisted in mixing of various metallic powders with different loading rates, injection moulding, followed by debinding and sintering of the components at different temperatures. This is also necessary to obtain proper replication of the components for the next analysis. For the final metallic replicas, the analysis has been conducted on shrinkage rate, density, surface roughness, Vickers hardness, and mass losses of mould cavities. The results finally demonstrate that the physical, mechanical properties and geometric dimensions of final replicas are affected by the powder nuance, solid loading rate and sintering temperature. It is therefore possible to manufacture components with the desired shapes, dimensions, physical and mechanical properties using the MIM process chain.

2 Materials and methods

2.1 Materials

The starting materials were commercially available. Gas atomised 316 L stainless steel powder (Osprey Ltd., UK) with an average particle size of 3.5 and 16 µm respectively and Fe–Ni powder are provided by Eurotungstene Company® (Eramet). The characteristics of these powders are reported in Table 1. Figure 2 shows SEM micrographs of the particles. As seen, the stainless steel particles are almost spherical whilst Fe–Ni particles are irregular. No evidence of severe powder agglomeration was observed during the SEM observation. Before mixing, the powders were dried in an oven at a temperature equal to 120 °C during 4 h in order to remove any moisture.

In our study, a binder system consisting of three components: polypropylene (PP; Goodfellow®), paraffin wax (PW; VWR Prolabo®) and stearic acid (SA; Sigma-Aldrich®), was used. A constant and appropriate formulation of the binder components was chosen according to the research of Quinard et al. [14] (Table 2). The binder composition and the characteristics of its components are given in Table 2. The binder is composed of waxes as the major component, SA as surfactant and PP as backbone polymer. The amount of surfactant was kept at relatively low value (<5 wt.%) to reduce the possibility of powder–binder separation due to an extra low viscosity of the binder system. Since wax and PP have certain degree of solubility, the amount of PP in the mixture is important as improper mixture exhibits two-phase flow behaviour with poor compatibility. As an illustration, Table 2 gives a typical mixed binder system well suited for the thermal debinding.

Table 2 Binder components and their characteristics

Binders	Melt temperature (°C)	Degradation temperature (°C)	Density (g cm^{-3})	Content (vol.%)
Polypropylene	160	360–450	0.90	40
Paraffin wax	58	210–340	0.91	55
Stearic acid	68	180–260	0.89	5

2.2 Elaboration of feedstocks and rheological characterisation

To prepare the different feedstocks, the binders and different metallic powders have been mixed in a Brabender® mixer with a pair of rotor blades (Fig. 3). In order to ensure adequate time for the binder to melt and homogenise, the binder components were initially blended at 170 °C in a mixer for 20 min. This temperature is within the highest melting temperature (160 °C) and the lowest degradation temperature of the binder system (180 °C). This allowed complete melting and prevented binder degradation. During mixing, the binder system was fed in first, followed by the

Fig. 3 The mixing equipment and its internal structure for mixing test

addition of powder in small consecutive loadings to achieve homogenous mixtures. When the mixing torque curve reaches a steady state and stable value, it means that the mixture is uniform. Then the feedstock is granulated into small pellets at room temperature for the replication by injection moulding. The composition of investigated feedstocks is listed in Table 2. The rheological characteristics of the feedstock were examined on a Bohlin® capillary rheometer. The shear rates of 10^2 to 10^4 s^{-1} were applied using a die with 1 mm diameter (D) and 16 mm length (L), giving a ratio (L/D), Eq. 16. Three different temperatures of 180, 200 and 220 °C were used.

2.3 Injection moulding

The granulated feedstocks have been injection moulded into the desired shape on an ARBURG horizontal injection moulding machine. The appropriate injection processing parameters were chosen for all the feedstocks (Table 3). A mould with a series of square pyramidal-shaped cavities was made by the electro-discharge machining (EDM) process (Fig. 4a). This micro-structured die insert had a mould cavity with dimensions of 3×3×0.8 mm, and its morphology was examined by a mechanical profilometer (Tencor-Alpha Step IQ) with a diamond tip measuring 5 μm in radius operated with a scanning speed of 5 μm/s (Fig. 4b, c).

2.4 Debinding and sintering

Firstly, the debinding was performed at 300 then 500 °C in an oven. The embossed parts were placed on an Al_2O_3 substrate. The debinding temperature used was based on the thermogravimetric analysis (TGA) curve for the binder system. As the SA and PW finish to degrade at about 350 °C, the first debinding temperature used was 300 °C. The temperature was then gradually increased to 500 °C corresponding to the curve that finally leads to an important weight loss of polypropylene and to the removal of all residual binder. The first debinding step removes part of the binders to obtain porous parts (called brown parts). The debound parts (brown parts) undewent a heat treatment for densification by solid state diffusion under vacuum in a graphite thermal furnace to consolidate them. After complete elimination of the binders, the temperature in the furnace would be continuously increased with a heating rate equal to 10 °C/min (Fig. 5). During this stage, the growth of contacts between metallic particles and their coalescence has been produced and the pores decreased and disappeared gradually in the samples. At last the densification was achieved at final sintering temperatures (from 1,150 to 1,360 °C) after a holding time of 1 h and the desired metallic parts were obtained.

Table 3 Injection moulding parameters in this work

Injection parameters	Injection temperature	Holding pressure	Holding time	Injection speed
Values	220 °C	180 MPa	20 s	20 mm^3/s

3 Results and discussion

3.1 Thermal properties

The degradation temperature ranges for the binder components in the powder-binder feedstocks have been obtained by TGA performed using a Setaram Setsys analyser®. Figure 6 records the TGA curves of polypropylene, SA and PW in the range from 20 to 500 °C with a heating rate equal to 5 °C/min. In Fig. 6, it is demonstrated that the SA, PW and polypropylene start to decompose at a temperature above 180, 210 and 360 °C, respectively. According to the TGA curves, the full degradation process occurs in the range from 180 to 340 °C for PW and SA and from 360 to 450 °C for the PP. When the test temperature is above 450 °C, the mass loss percentage of the three materials tends to 0 % at higher temperature, which is the ideal case for binder removal in the debinding of MIM part.

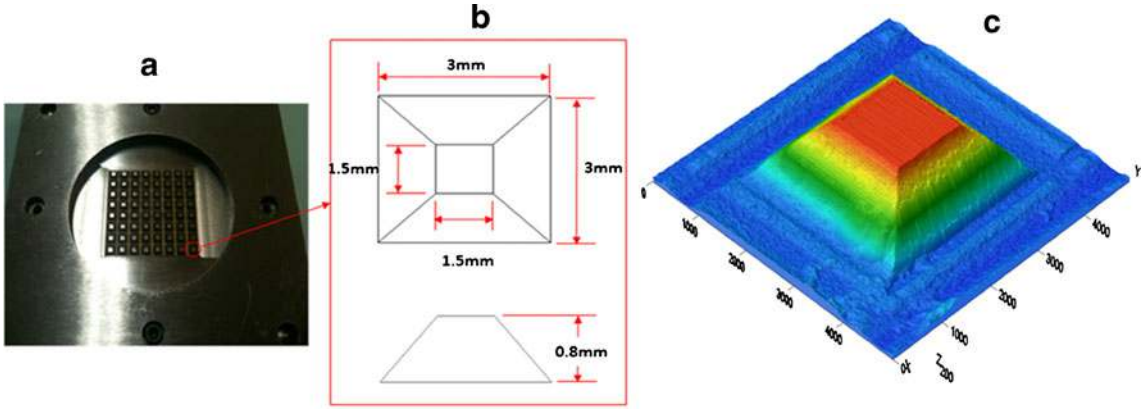

Fig. 4 **a** Photograph of **a** micro-structured die mould made using EDM, **b** dimensions of pyramid-shaped cavity and **c** 3D topography image of the original metallic mould

The main goal of mixing is to produce a homogeneous feedstock with suitable rheological behaviour for subsequent processing steps. The thermogravimetric results in Fig. 7 show that the obtained feedstock after mixing process is almost homogeneous since the corresponding thermogravimetric curves are well superimposed. Additionally, the standard deviation of the binder losses for the manufactured feedstock is 1.10×10^{-2} wt.%. Stainless steel feedstock had three significant mass loss stages with increasing temperatures (see Fig. 7). The three onset temperatures at 180, 210 and 340 °C were due to the degradation temperatures of SA, PW and PP, respectively. Above 450 °C, all binder components were burned off. Hence, based on the TGA result, a multi-step debinding profile was established to remove progressively the multi-component binder system. The progressive debinding over a wide temperature with proper heating rate could retain the part integrity and prevent the formation of debinding defects, such as blister, cracking and slumping. The homogeneity of the feedstock after the mixing stage was also examined under a scanning electron microscope (Fig. 8).

3.2 Elaboration of feedstocks and rheological characterisation

In this work, several feedstocks with different metallic powders and different solids loading are prepared by a mixing process. Figure 9 shows the mixing behaviour of 316L stainless steel powders with loading ratio from 56 to 64 vol.% (3.5 μm particle size). The mixing torque, proportional to the shear stress of the mixer, indicates that the work energy was consumed to disperse and distribute the powder in the binder. The torque value increases as the solid loading varies from 56 to 64 vol.% due to the higher resistance generated by higher powder content. For each of the 56 and 64 vol.% solids loading, the torque stabilises at a steady level in a short time indicating uniform mixing.

Figure 10 shows the results obtained with the capillary rheometer in term of shear viscosity vs. shear rate curves of the mixed feedstocks tested at different temperatures. The data indicate the flowability of MIM feedstocks, for which, the lower value of viscosity shows the easier flow of feedstock. According to the viscosity curves related in Fig. 10, the viscosity of the feedstock decreases with the increase of shear rate and temperature, indicating pseudo-plastic flow

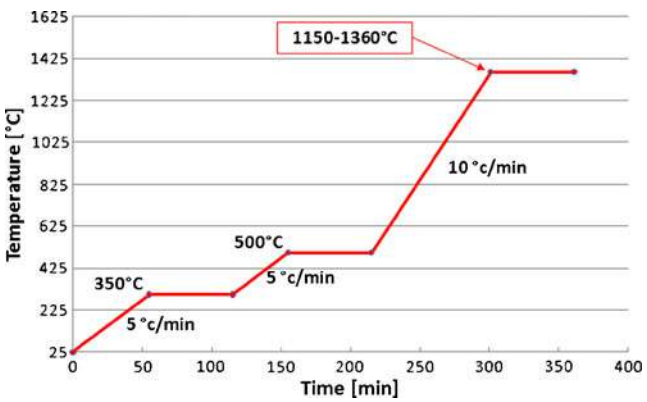

Fig. 5 Debinding and sintering kinetic cycle used for debinded components

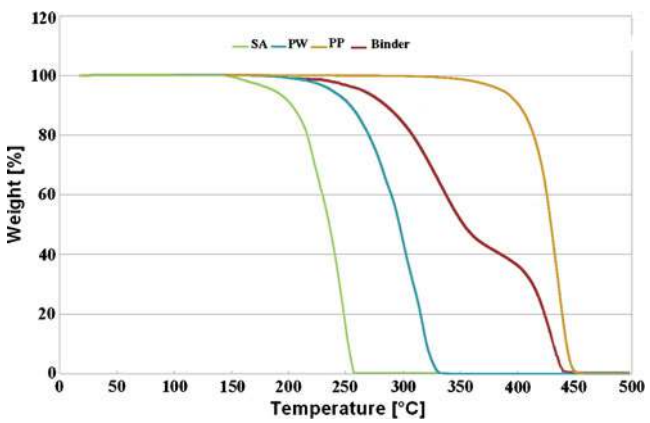

Fig. 6 The TGA analyses of the binder system

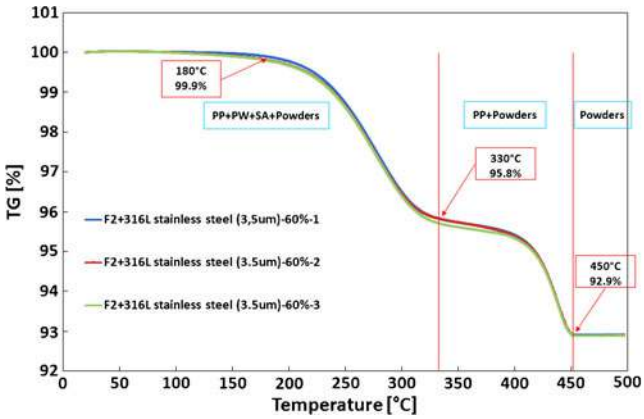

Fig. 7 TGA curves of the 316L stainless steel feedstock with a 60 vol.% powder (paticle size equal to 3.5 μm) loading

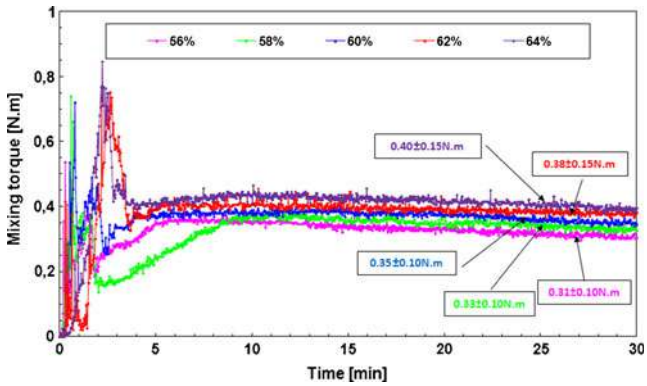

Fig. 9 Mixing torques vs. time of 316L stainless steel feedstocks (3.5 μm) obtained at different volumetric loading, using 30 min and 30 rpm at 170 °C

behaviour. Normally, feedstock exhibiting pseudo-plastic flow during injection facilitates cavities filling.

3.3 Dimensional change and shrinkage

During thermal debinding and sintering, moulded parts undergo binder elimination and subsequently particle bonding, which results in dimensional change in the parts. Generally, the dimensional change of a part is described by the anisotropic shrinkage between the moulded and the sintered parts. Figure 11 shows the photographs of the metallic replicas at different processing steps. The metallic replicas were well replicated from the mould insert. Macro-defects, such as warpage, blister, etc. were not visible in the moulded, debound and sintered metallic replicas.

The dimensional shrinkage of replicas after sintering process was clearly evident, whilst the dimensional change was not noticeable after debinding. The shrinkage of the metallic replicas is show in Table 4 (all the demonstrated values are the averages of measured values for ten times). The measure of thickness/diameter changes of the metallic replicas obtained with a vernier caliper, were much closer, at about 11–15 %, which was a typical value for MIM parts. The shrinkage percentages of width and depth of the micro-sized pyramid-shaped structure, probed with a mechanical profilometer, were 14–23 %. Evidently, the shrinkage of the micro-sized pyramid-shaped structure is directly depending on several factors such as powder nuance, loading rate, particles sizes and sintering temperature (see Fig. 12a, b).

In the debinding process and the first stage of the sintering process (25–500 °C), all the polymeric binders in the injected replicas have been completely eliminated and some pores have been created in the replicas as a result of the elimination of the binders; moreover, the sintering necks started to form between the metallic micro-particles which prevent the movement of the micro-particles and then keep the original dimensional shape and the topographic features of the injected replicas. In the second stage of sintering (500–1,150/1,360°C), the temperature in the furnace continuously increased up to the final densification temperatures (in this work, it is from 1,150 to 1,360 °C) and has been maintained for a period (1 h) to ensure adequate densification of the micro-particles; during this stage, the internal metallic powder particles exhibit coalescence and bonding behaviour, as well as take the place of the pores, then the

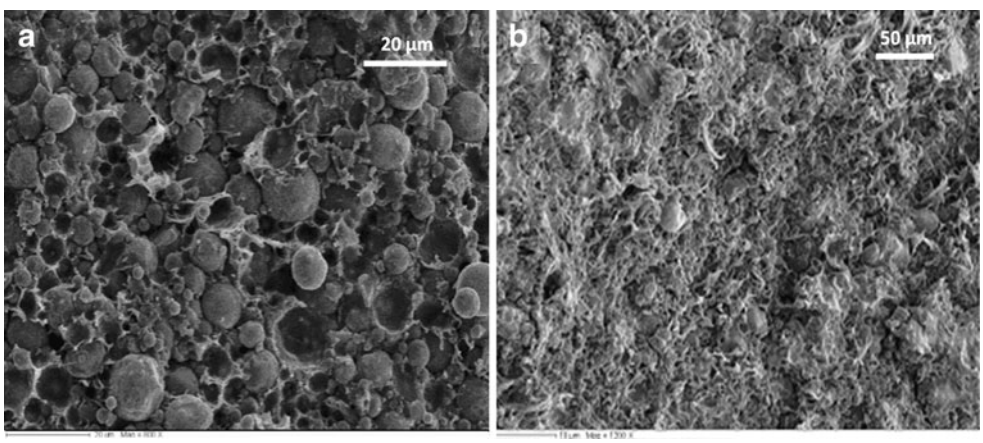

Fig. 8 SEM photographs of the feedstock on 316L stainless steel powders (16 μm) (**a**) and Ferronickel powders (**b**) (powder volume loading is 60 %) after mixing during 30 min at 170 °C

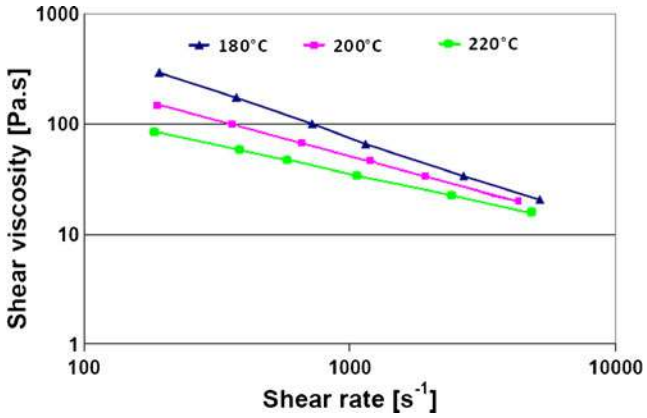

Fig. 10 Shear viscosity vs. shear rate corresponding to 316L stainless steel (3.5 μm) feedstock with loading ratio equal to 60 vol.%, at different temperatures

densification of metallic powders is carried out. Therefore, an evident dimensional change and shrinkage of replicas are produced. In this study, scanning mechanical microscopy (SMM) has been used to estimate the dimensional and geometrical qualities of densified replicas by measuring and comparing the shapes of 2D profiles extracted from the die cavities of the imprinted moulds.

For investigating the influence of the solid loading ratio, sintering temperature and the nuance of powder particles to the shrinkage of sintered replicas, SMM has been used to obtain the 2D profiles of the metallic replicas (all the measurements have been executed four times at five random cavities, and the demonstrated results are the average values). The 2D profiles of the replicas with the 316L stainless steel powders (3.5 μm particle size) feedstock of solid loading in volume ranging from 56 to 64 % and sintered at 1,150 °C have been measured and compared. It is observed that the shrinkage of the sintered cavities is in range from 15 to 22 % and the profile of the cavity fabricated with feedstock at loading of 56 % has the largest shrinkage and that of 64 % has the smallest shrinkage. As a result, one can conclude that the shrinkage rate of the replicas decreases with increasing solid loading. Besides, in order to investigate the effect of the final sintering temperature on the dimension of the replicas, the 2D profiles of the replicas sintered at different final sintering temperatures in the range from 1,150 to 1,360 °C with the feedstock of 60 % 316L stainless steel powder (3.5 μm particle size) have been also measured and compared. In Fig. 12a, it can be observed that the size proportion of the sintered cavities relative to the original cavity has a trend to decrease with the increase of the sintering temperature, which means that a higher sintering temperature can increase effectively the shrinkage rate of the replicas. The same method has been also used for investigating the influence of the nuance of powder particles (particle shapes and diameters) on the dimensional change, where the different 2D profiles of replicas sintered at 1,250 °C with different metal powder feedstocks having the same solid loading of 58 % have been compared. It is found that the replica of Fe–Ni (8 %; with irregular particle shape and 5 μm particle size) has a shrinkage rate (20–22 %) larger than that of 316L stainless steel (spherical particles of 3.5 μm size; 18–20 %), and the replica of 316L stainless steel (spherical particles of 16 μm size) has the smallest shrinkage (15–17 %). Therefore, a conclusion can be obtained: with the same process conditions, the micro-powder particles with smaller size and with irregular shape lead to larger shrinkage for the sintered replica fabricated by MIM.

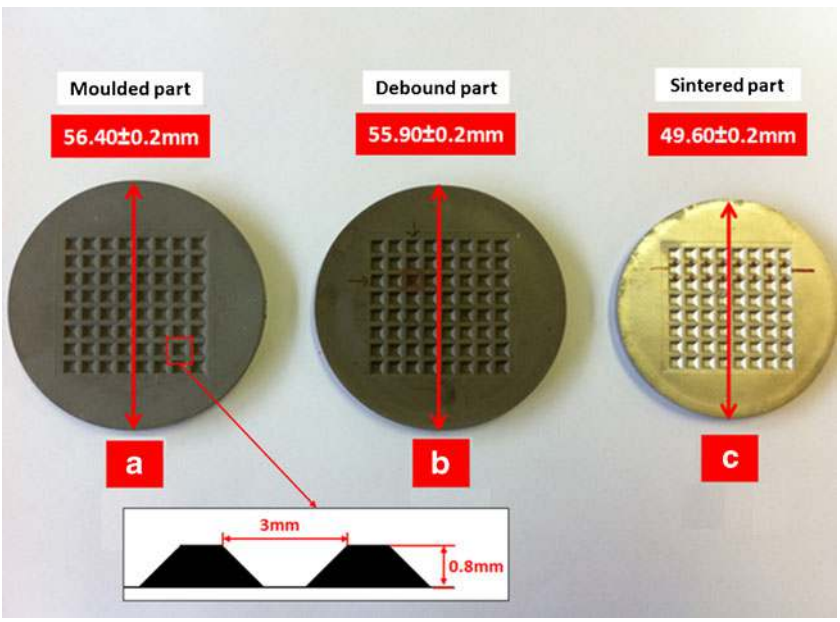

Fig. 11 Photographs of the stainless steel replicas after different processing steps: **a** moulded to 220 °C, **b** dedinded up to 500 °C and **c** sintered up to 1,150 °C

Table 4 The size details of die mould and micro-sized structures of metallic replica

Die mould insert				Stainless steel replicas sintered at 1,200 °C with powder volume loading equal to 62 % (D_{50}=3.4 μm)			
Diameter (mm)	Thickness (mm)	Pyramid-shaped structures		Diameter (mm)	Thickness (mm)	Pyramid-shaped structures	
		Width (mm)	Height (mm)			Width (mm)	Depth (mm)
57±0.2	4±0.1	3±0.01	0.8±0.01	46.7±0.2	3.2±0.1	2.4±0.01	0.6±0.01

For the MIM process, the homogeneity is an import standard to evaluate the sintering quality of replicas. In order to investigate the homogeneity, the shrinkage rate of replicas in different directions has been measured and compared; a replica sintered at 1,200 °C on 316L stainless steel powder (3.5 μm particle size) with a loading rate of 60 % has been chosen and scanned in the *X*–*X* and *Y*–*Y* directions (Fig. 12b) by using SMM. The scanning results show that the 2D profiles of every cavity in both directions are approximately identical which means that the shrinkage of the replica is uniform in the *X*–*X* and *Y*–*Y* directions during the MIM process. The measured shrinkage rate is within the range 15 to 20 %; besides the shrinkage in the thickness direction (*Z*–*Z*) has also been measured, but its rate is within the range 20 to 25 %. The results indicate that the replica undergoes an isotropic shrinkage in the radial direction and an anisotropic shrinkage in the radial direction and in the thickness direction. Moreover, a total mass loss around 20 % is measured compared with the injected replica. Even though there is shrinkage of replica during the debinding and sintering processes, the dimensional change could be almost compensated by the design of the mould cavity.

3.4 Surface roughness

Roughness measurements were carried out on the cavities of the debound replicas manufactured from different metal powders with different loading rates and the same replicas

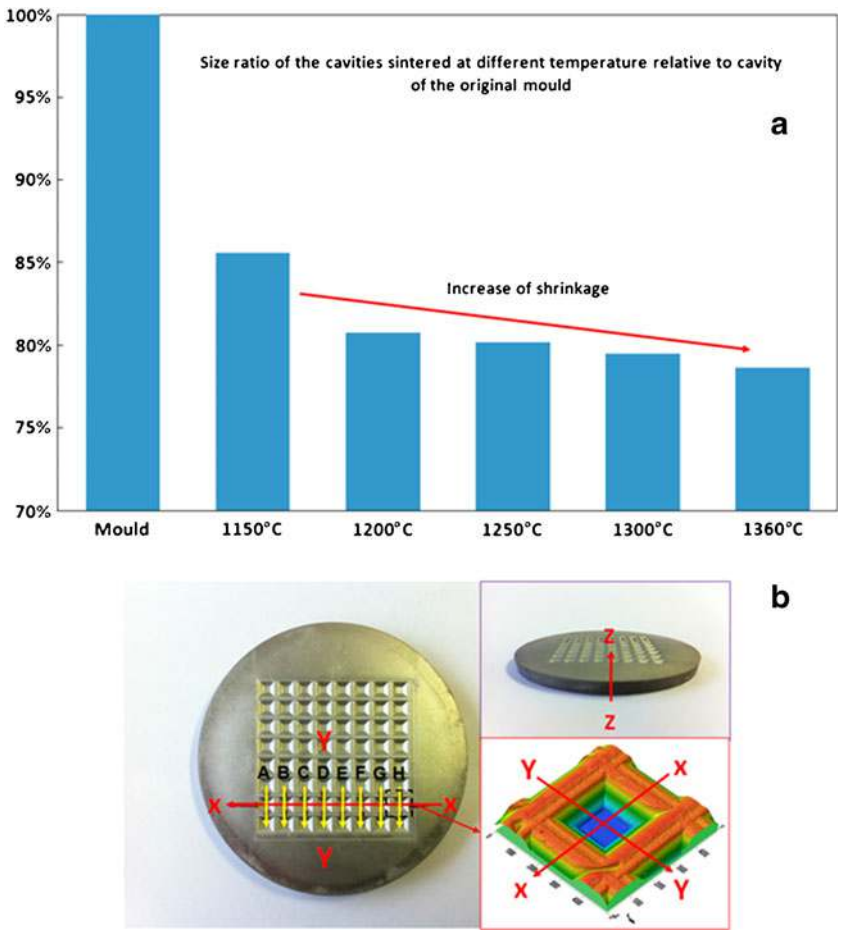

Fig. 12 Shrinkage of the pyramid-shaped structures of metallic replicas fabricated with the feedstock loaded with 62 vol.% of 316L stainless steel powder (3.5 μm), sintered at different temperature (**a**) and the testing directions of homogeneity tests for sintered replicas (**b**)

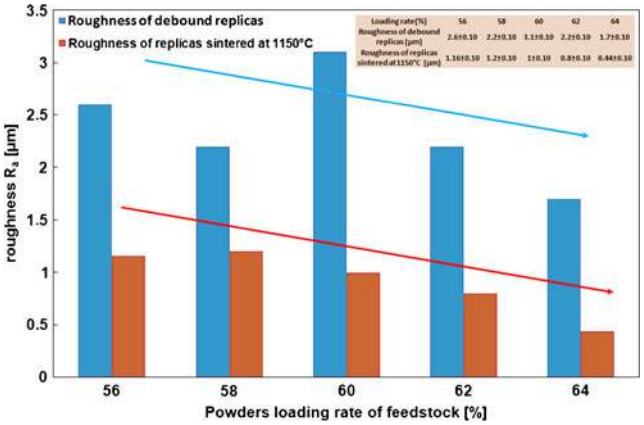

Fig. 13 Evolution of roughness R_a depending on the loading rate for the replicas debound and sintered at 1,150 °C

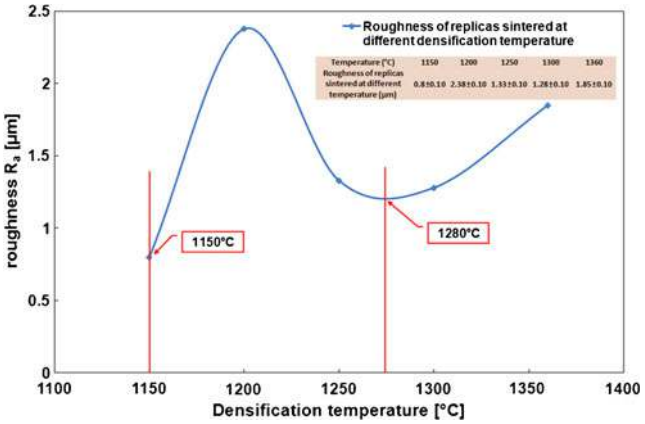

Fig. 15 Evolution of roughness R_a depending on the densification temperature for the replicas loaded with 62 vol.% of 316L stainless steel powders (3.5 µm)

sintered across a wide range of temperatures and all the measurements have been executed four times at five random cavities. Through the comparison of the measurement average values, it is observed that: (1) the surface roughness of debinded replicas is higher than that of sintered ones, the densification of powder particles improves the surface quality of replicas; (2) at the same final sintering temperature, the surface roughness of sintered replicas decreases with the increase of the metal solid loading (Fig. 13), because the high loading of the powders helps to reduce the pores in the replica and improves the densification ability of metallic powders; (3) for the replicas with the same solid loading and sintered at the same temperature, their surface roughness depends on the nuance of the metal powders, the finer powders corresponding to the lower roughness value. However, irregular powder particle shape did not demonstrate evident influence on the roughness of sintered replicas, while for the debound replicas, irregular particle shape results in lower roughness (Fig. 14); (4) the roughness evolution of replicas sintered at different temperature with the same type of powder and loading rate is not a simple linear

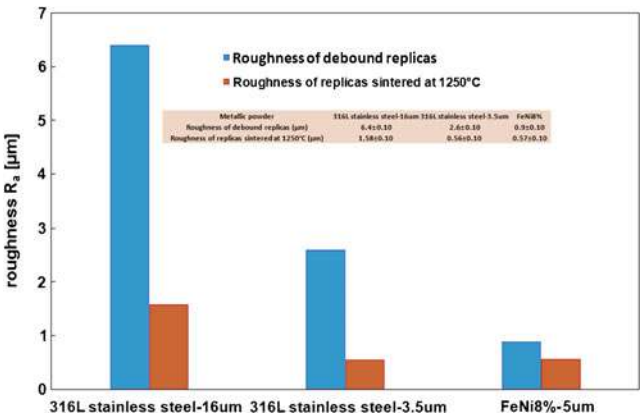

Fig. 14 Evolution of roughness R_a depending on the nuance of powders for the replicas debound and sintered at 1,250 °C

function of the densification temperature. Figure 15 shows that the lower roughness can be obtained at about 1,150 and 1,280 °C.

3.5 Density and hardness evolutions

The densities of all the sintered metallic replicas have been measured by hydrostatic weighing (the demonstrated results are the average values of five times measuring for three different replicas). According to the ratio between the mass of the replica in air and its mass in a fluid (pure ethanol), the hydrostatic density can be calculated by using the Eq. 1. Figure 16a, b is related to the results of the measured density for the replicas of 316L stainless steel powder (3.5 µm) and shows respectively the evolution of the density depending on the densification temperature and along with the solid loading. It is observed that the density of sintered replicas (with the same loading rate of 62 %) increased from 7.52 to 7.67 g/cm^3 when the sintering temperature increased from 1,150 to 1,360 °C, and the maximum density (sintered at 1,360 °C) is almost equal to 97 % of 316L stainless steel theoretical density; when the solid loading increased from 56 to 64 %, the density of replicas (sintered at 1,250 °C) increased from 7.24 to 7.64 g/cm^3, the maximum density is equal to 96 % of the theoretical density. Wherefore, one can conclude that: the increase of solid loading and raising of densification temperature can improve effectively the density of sintered replicas. The measured densities of replicas manufactured from 316 stainless steel powder (16 and 3.5 µm particle sizes) and Fe–Ni (5 µm particle size) with the same loading rate of 58 % sintered at 1,250 °C are reported in Fig. 17. The results show that the replicas made from 316L stainless steel powders and Fe–Ni (8 %) achieve respectively 91, 93 and 96 % of their theoretical densities. The influence of powder particles size and shape was demonstrated clearly: the small size and irregular shape of

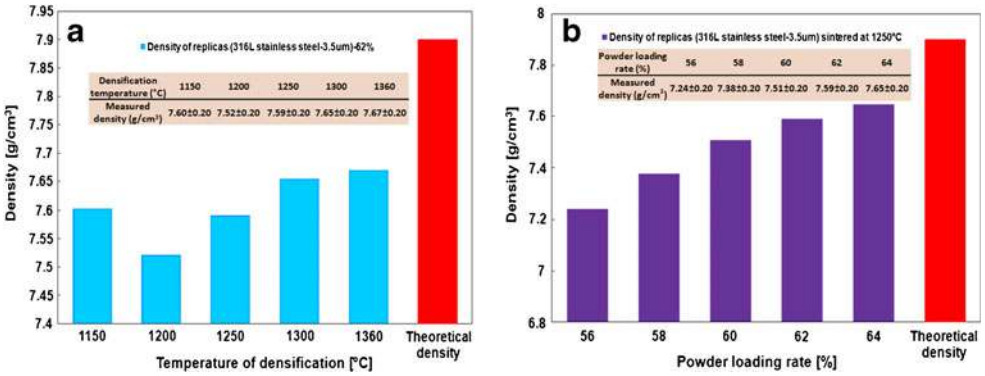

Fig. 16 Evolution of density for replicas of 316L stainless steel powders (3.5 μm particle sizes) sintered **a** at different densification temperature, using 62 % solid loading in volume, **b** at 1,250 °C with different loading rate

particles help to produce replicas with a higher density during the sintering process.

$$\rho_{\mathbf{hyd}} = W_{\mathbf{air}} \times \mathbf{0.7888}/(\mathbf{0.99983} \times (\mathbf{W_{air}} - \mathbf{W_{fluid}}) - \mathbf{0.0012}) \quad (1)$$

Hardness is also considered as an important index to evaluate the mechanical properties of a metallic component. In our study, the Vickers hardness on the polished cross-section area of the sintered replicas has been measured and analysed. In our measurements, the applied loading weight on the test area of the sintered replicas was 10 kg and the holding time was 10 s; five tests have been performed at a different position for all the samples; the average values has been calculated; and the final results are illustrated in Figs. 18a, b and 19. Figure 18a shows the effect of the densification temperature on Vickers hardness of sintered replicas fabricated with 62 vol.% of 316L stainless steel powders (3.5 μm); as the densification temperature increases from 1,150 to 1,360 °C, the hardness increases from 163 to 180 Hv; therefore, one can conclude that raising the densification temperature can effectively enhance the Vickers hardness of sintered replicas. Figure 18b demonstrates the Vickers hardness of replicas sintered at 1,150 °C with different solid loading (from 56 to 64 %); it is observed that the change of the solid loading did not influence regularly the Vickers hardness of sintered replicas. Moreover, the hardness of replicas manufactured from 316L stainless steel powders with different average particle diameters of 3.5 and 16 μm has also been compared in Fig. 19. In conclusion, the finer metallic powders can increase the Vickers hardness of the sintered replicas. In order to research the homogeneity of the hardness of the sintered replicas, a new measurement has been conducted: 9 points have been chosen as the test points respectively in the horizontal and vertical directions on the polished cross-section area of the sintered replicas (Fig. 20); the measurement of the Vickers hardness has been conducted at these points. According to the results demonstrated in Fig. 21, one can conclude that the hardness of the sintered replica is not homogeneous and that the hardness increases gradually from the edge to the centre of the replica along the radial direction.

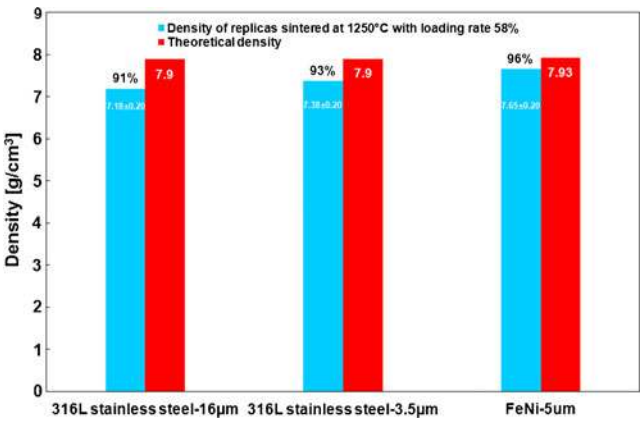

Fig. 17 Comparison of density for replicas loaded with different powders with same loading rate (58 vol.%) and densification temperature (1,250 °C)

4 Conclusions

In this paper, a complete fabrication chain to manufacture the structured metallic die mould with micro-metallic powders: 316L stainless steel (16 μm; 3.5 μm particles size) and Fe–Ni (8 %; 5 μm particles size) by replication technology —MIM has been presented; numerous metallic die moulds haven been successfully obtained by using the feedstocks (powders/binders) loaded with different micro-powders using different sintering conditions; the possibilities to obtain the structured replicas with desired properties by MIM has been proved. Large number of experiments has been carried out and scientific statistic method has been applied to analyse the evolution of the physical and mechanical properties of a die mould manufactured by MIM as well as the different factors influencing these properties in the MIM process.

In the first stage, all the ingredients in the binders system have been analysed to determine the proper range of temperature for the mixing, injection moulding and debinding processes by TGA; next, the feedstocks with different solid

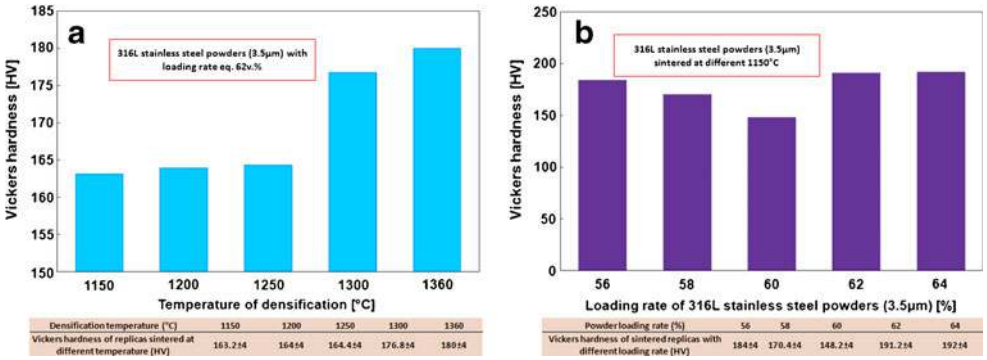

Densification temperature (°C)	1150	1200	1250	1300	1360
Vickers hardness of replicas sintered at different temperature (HV)	163.2±4	164±4	164.4±4	176.8±4	180±4

Powder loading rate (%)	56	58	60	62	64
Vickers hardness of sintered replicas with different loading rate (HV)	184±4	170.4±4	148.2±4	191.2±4	192±4

Fig. 18 Vickers hardness evolution of metallic replicas sintered **a** at different temperatures **b** with different loading rates

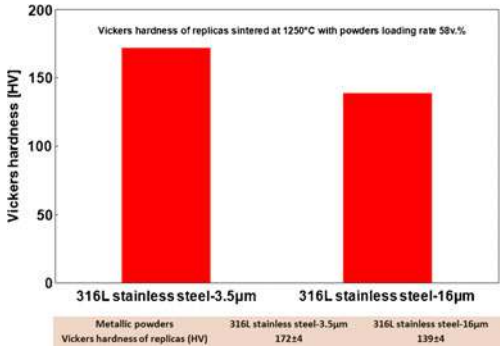

Metallic powders	316L stainless steel-3.5μm	316L stainless steel-16μm
Vickers hardness of replicas (HV)	172±4	139±4

Fig. 19 Vickers hardness comparison of metallic replicas with different powder particle sizes

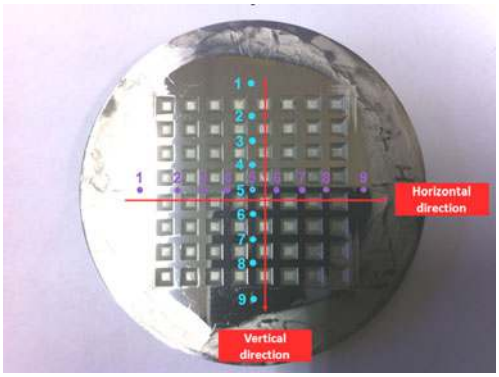

Fig. 20 Position distribution diagram of the chosen test points

loading from 56 to 64 % for injection moulding have been prepared by a mixing process. The influences of solids loading on the mixing torque has been demonstrated; the flowability of the MIM feedstock has been investigated; then, the prepared feedstocks have been used to produce the structured replicas (die mould) by injection moulding with the suitable forming parameters; after the injection moulding process, all the injected replicas have been debound to eliminate the binders following the same kinetic cycle, but the sintering processes have been conducted at five different densification temperatures to achieve the densification of the metallic powders for the debound replicas. After the sintering process, the final metallic structured replicas (die mould) were obtained by MIM.

In the second stage, the physical and mechanical properties of sintered replicas have been measured and tested. Through the comparison of the 2D profiles of cavities of sintered die moulds, a shrinkage of 12–21 % compared with the injected replicas has been observed; the results showed that increasing the powders loading rate can reduce the shrinkage of the sintered replicas; the replicas fabricated by using the powders with finer particles and irregular shapes have larger shrinkage; and the shrinkage of sintered replicas was isotropic in the radial direction but anisotropic between the radial and thickness directions. The measurement of the roughness, density and hardness of different sintered replicas demonstrated that high solid loading rates and irregular fine powders can effectively strengthen the qualities of the sintered replicas: increase of the density as

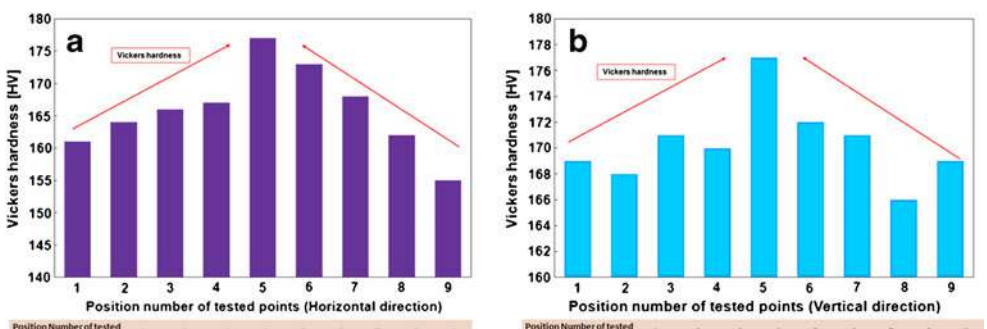

Position Number of tested points (Horizontal)	1	2	3	4	5	6	7	8	9
Vickers hardness (HV)	161±4	164±4	166±4	167±4	177±4	173±4	168±4	162±4	155±4

Position Number of tested points (Vertical)	1	2	3	4	5	6	7	8	9
Vickers hardness (HV)	169±4	168±4	171±4	170±4	177±4	172±4	171±4	166±4	169±4

Fig. 21 Distribution of Vickers hardness of replicas along horizontal **a** and vertical **b** directions

well as hardness and reduction of the roughness; besides, a desired density of 316L stainless steel replicas which is approximately equal to 97 % of the theoretical density has been achieved.

Finally, the metallic die moulds with proper shape retention and without visible defects have been successfully fabricated by MIM; the factors (powders loading rate, powders particle shape and densification temperature) influencing the physical and mechanical properties of sintered replicas have been comprehensively studied and analysed; the possible direction to improve the qualities of the sintered replicas has been indicated.

Acknowledgement This work was performed within the framework of the French FUI CONPROMI project.

References

1. Ye H, Liu XY, Hong H (2008) Fabrication of metal matrix composites by metal injection molding—a review. J Mater Process Technol 200:12–24
2. Meng J, Loh NH, Fu G, Tay BY, Tor SB (2011) Micro powder injection moulding of alumina micro-channel part. J Eur Ceram Soc 31:1049–1056
3. Zauner R (2006) Micro powder injection moulding. Microelectron Eng 83:1442–1444
4. Loebbecke B, Knitter R, Haußelt J (2009) Rheological properties of alumina feedstocks for the low-pressure injection moulding process. J Eur Ceram Soc 29:1595–1602
5. Piotter V, Mueller T, Plewa K, Prokop J, Ritzhaupt-Kleissl H-J, Hausselt J (2010) Manufacturing of complex-shaped ceramic components by micropowder injection molding. Int J Adv Manuf Technol 46:131–134
6. Thomas-Vielma P, Cervera A, Levenfeld B, Várez A (2008) Production of alumina parts by powder injection molding with a binder system based on high density polyethylene. J Eur Ceram Soc 28:763–771
7. Checot-Moinard D, Rigollet C, Lourdin P (2011) Powder injection moulding PIM of feedstock based on hydrosoluble binder and submicronic powder to manufacture parts having micro-details. Powder Technol 208:472–479
8. Imgrund P, Rota A, Petzoldt F, Simchi A (2007) Manufacturing of multi-functional micro parts by two-component metal injection moulding. Int J Adv Manuf Technol 33:176–186
9. Ahn S, Park SJ, Lee S, Atre SV, German RM (2009) Effect of powders and binders on material properties and molding parameters in iron and stainless steel powder injection molding process. Powder Technol 193:162–169
10. Karatas C, Kocer A, Ünal HI, Saritas S (2004) Rheological properties of feedstocks prepared with steatite powder and polyethylene-based thermoplastic binders. J Mater Process Technol 152:77–83
11. Paisan S, Arada B, Sawai D (2008) The effects of binder components in wax/oil systems for metal injection molding. J Mater Process Technol 196:94–100
12. Olevsky EA (1998) Theory of sintering: from discrete to continuum. Mater Sci Eng R23:41–100
13. Meng J, Loh NH, Tay BY, Tor SB, Fu G, Khor KA, Yu L (2011) Pressureless spark plasma sintering of alumina micro-channel part produced by micro powder injection molding. Scr Mater 64:237–240
14. Quinard C, Song J, Barriere T, Gelin JC (2011) Elaboration of PIM feedstocks with 316 L fine stainless steel powders for the processing of micro-components. Powder Technol 208:383–389
15. Koseski RP, Suri P, Earhardt NB, German RM, Kwon Y-S (2005) Microstructural evolution of injection molded gas- and water-atomized 316 L stainless steel powder during sintering. Mater Sci Eng, A 390:171–177
16. Gutiérrez-López J, Rodriguez-Senín E, Pastor JY, Paris MA, Martín A, Levenfeld B, Várez A (2011) Microstructure, magnetic and mechanical properties of Ni–Zn ferrites prepared by powder injection moulding. Powder Technol 210:29–35
17. Ruh A, Piotter V, Plewa K, Ritzhaupt-Kleissl H-J, HauBelt J (2012) Studies on size accuracy of microgear wheels produced by powder injection molding of zirconia feedstocks. Int J Adv Manu Technol 58:1051–1059
18. M. Sahli, G. Larsen, T. Barriere, J.C. Gelin and G. Michel (2010) Analysis and characterization for 316L stainless metal microstructure replication of micro-components produced by micropowder injection moulding. Journal at Steel Research 123–132
19. Zhang SX, Chandrasekaran M, Li QF, Ho MK, Yong MS (2008) Studies on the fabrication of tool steel components with microfeatures by PIM. Int J Adv Manuf Technol 38:278–284
20. Li D, Hou H, Liang L, Lee K (2010) Powder injection molding 440C stainless steel. Int J Adv Manuf Technol 49:105–110
21. Khalil KA, Kim SW (2006) Relationship between binder contents and mechanical properties of 17–4 ph stainless steel fabricated by PIM process and sintering. Matels and Mater Int 12(2):101–106
22. Okubo K, Tanaka S, Ito H (2010) The effects of metal particle size and distributions on dimensional accuracy for micro parts in micro metal injection molding. Microsys Technol 16:2037–2041
23. Li Y, Li L, Khalil KA (2007) Effect of powder loading on metal injection molding stainless steels. J Mater Process Technol 183:432–439
24. Choi S-H, Kang S-D, Kwon YS, Lim SG, Cho KK, Ahn I-S (2010) The effect of sintering conditions on the properties of WC–10wt%Co PIM compacts. Res Chem Intermed 36:743–748